Journal of Materials Chemistry A

Accepted Manuscript

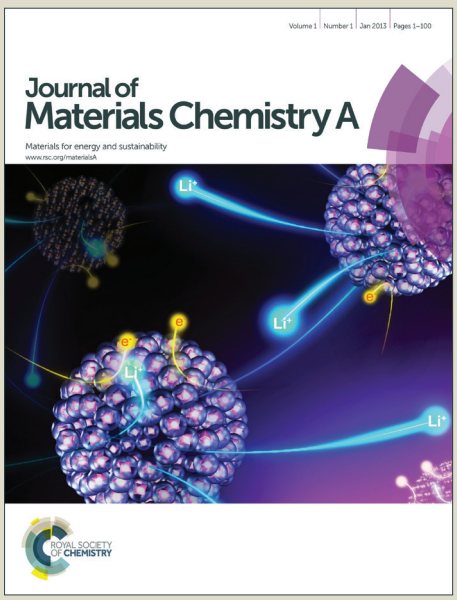

ROYAL SOCIETY OF CHEMISTRY

www.rsc.org/materialsA

Journal Name

RSCPublishing

COMMUNICATION

Synergistically engineered self-standing silicon/carbon composite arrays as high performance lithium battery anodes

Cite this: DOI: 10.1039/x0xx00000x

Bin Wang, Tengfei Qiu, Xianglong Li,* Bin Luo, Long Hao, Yunbo Zhang and Linjie Zhi*

Received 00th January 2012,
Accepted 00th January 2012

DOI: 10.1039/x0xx00000x

www.rsc.org/

The synergistically engineered self-standing silicon/carbon composite arrays exhibit unprecedented lithium storage performance, including high specific capacity of 1510 mAh g^{-1} based on the total electrode weight, extraordinary cycling stability with nearly 100% capacity retention over 600 cycles, and areal capacity approaching the value of commercial lithium-ion batteries (3.9 mAh cm^{-2}).

Silicon is considered as an attractive anode material for next-generation lithium-ion batteries due to its relatively low working potential, abundance in nature, and more importantly highest known theoretical capacity (3579 mAh g^{-1} for $Li_{15}Si_4$ at room temperature) which is about ten times that of commercial graphite anodes.[1] However, silicon electrodes suffer from severe capacity fade upon cycling. The capacity fade is attributed to structural degradation and the instability of solid electrolyte interphase (SEI) on the surface caused by the tremendous volume change of silicon (up to 300%) during lithiation and delithiation processes.[2] One popular tactic to address this issue is to combine nanostructured silicon with a second phase (e.g., carbon).[3-10] Notably, to encapsulate nanostructured silicon in a hollow carbon shell and subsequently construct conventional slurry-based electrodes represents a state-of-the-art electrode design strategy, featuring many advantageous characteristics (Design I at low mass loading, Fig. 1). As the nanostructured silicon is able to withstand the large lithiation/delithiation-induced strains without fracture, the hollow carbon shell enables the creation of an internal void space to accommodate the volume change of silicon, and also functions as an electrolyte blocking layer to prevent the direct contact of electrolyte and silicon and thus improve the surface stability of the material. Accordingly, diverse examples have been recently demonstrated such as Si/C yolk-shell and wire-in-tube nanocomposites,[11-15] yielding remarkable improvement in cycle lives. Unfortunately, long-term stable cycling with high capacity has been registered always based on low areal mass loadings (typically, <0.2 mg cm^{-2}). This leads to low areal capacity as encountered in early silicon thin-films,[16] which has long been recognized to be a fatal problem of hindering the implementation of silicon in a viable lithium-ion battery.[17-19] As the buildup of micro-sized Si anode materials with nanoscale building blocks[20,21] have been shown to be an effective way to tackle this problem, it still remains challenging to achieve long-term stable cycling at high areal capacity. Such a situation holds as well for many other nanostructured silicon and electrode materials subject to large volume change.

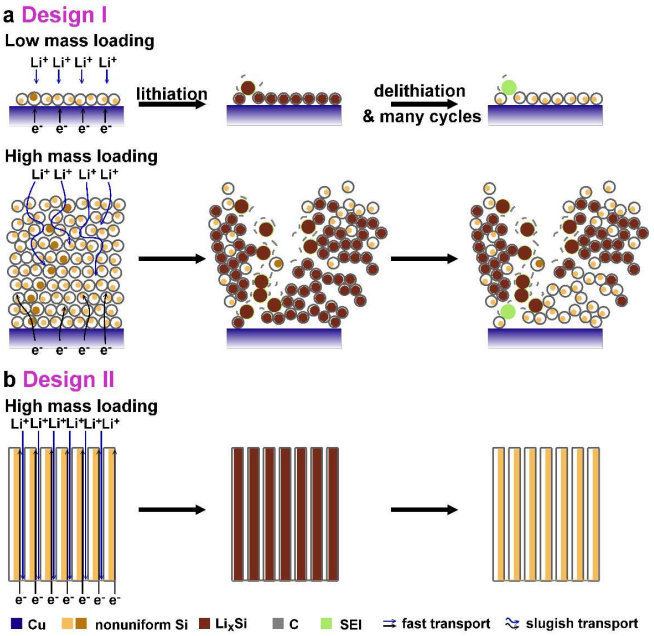

Fig. 1 Schematic illustration of (a) Design I and (b) Design II. Compared to the Design I with nanostructured silicon encapsulated in a hollow carbon shell and subsequently constructed into a conventional slurry-based electrode, the Design II demonstrated here features synergistic engineering and control of structure, interface, and charge transport of the electrode; specifically, the uniform Si/C

wire-in-tube nanostructuring promises the structural and interfacial stabilization of each resultant Si/C nanocomposite and promotes electrode-level homogeneity, and the self-standing array manufacturing allows easy access of both electron (e^-) and lithium ion (Li^+) to every Si/C building block even at high areal mass loading.

There exist two main causes of adopting the low areal mass loading of nanostructured materials (Design I, Fig. 1). First, compared with bulk and micrometer-sized materials, the use of nanostructured materials generally introduces excessive and highly disordered interparticle interfaces,[22] over which the binders and other additives involved in a conventional electrode configuration cannot consistently enable the creation of continuous and fast transport pathways for either electrons, or lithium ions, or both, as the areal mass loading increases and the electrode thickens. Second, upon cycling, the nonuniformity of nanostructured materials induces structural changes locally upon cycling, which can accumulate across the electrode thickness, thus incurring the electrode-level cracking and failure.[19,23] Compared with a thin electrode with low areal mass loading, it can be expected that a thick electrode at high areal mass loading is much more susceptible to as-accumulated variations. In line with the above considerations, to deposit nanostructured silicon uniformly on ordered one-dimensional conductive scaffolds (e.g., copper, nickel) can be an encouraging design strategy, because such structured design paradigm not only offers uninterrupted (that is, nearly interface resistance-free), vertical, and fast electron and ion transport highways for every individual material building block, but also provides flexibility in electrode thickness based upon the facile tailoring of conductive substrates and/or scaffolds, rather than the addition of supplementary binders and additives. Sticking to such design formula, different conductive substrate-based electrode prototypes have already been successfully demonstrated.[24-30] However, stable cycling (e.g., 100 cycles) with areal capacity comparable to the level of commercial lithium-ion batteries has rarely been reported, which is fundamentally due to the lack of sufficient control of structural and interfacial instabilities of silicon during cycling. So far, it still remains very challenging to harness the lithium storage capability of nanostructured materials (e.g., silicon in this work) specifically at an acceptable mass loading level, and new design protocols are thus highly desirable.

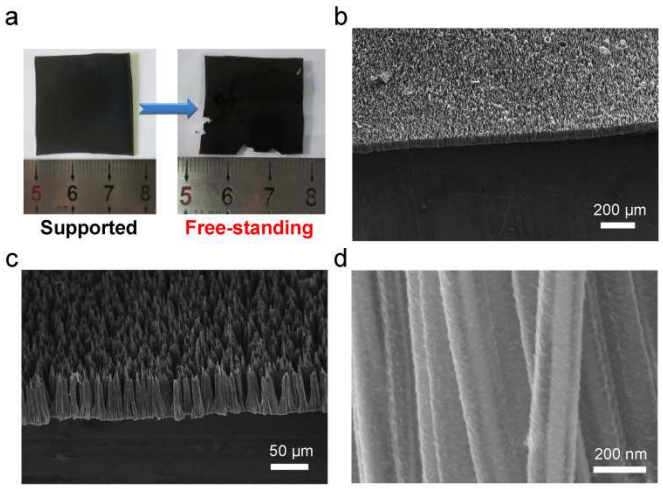

Fig. 2 The morphology of wt-Si/C arrays: (a) Photographs of a wt-Si/C array before and after being peeled off from the substrate; (b-d) Scanning electron microscopy (SEM) images of a wt-Si/C array.

Here, we propose a novel design (Design II, Fig. 1) for large volume change lithium battery anodes by synergistic engineering and control of structure, interface, and charge transport of the electrode. As a proof-of-concept model, the resulted self-standing, ordered arrays of uniform Si/C wire-in-tube nanocomposites (namely, wt-Si/C arrays) are endowed with two major features. First, the uniform Si/C wire-in-tube nanostructuring guarantees the structural and interfacial stabilization of each counted wt-Si/C building block and promotes electrode-level homogeneity. Second, the free standing array manufacturing allows easy access of both electrons and lithium ions to every wt-Si/C nanocomposite building block even at high areal mass loading. As a result, the wt-Si/C arrays exhibit unprecedented lithium storage performance at substantially enhanced areal mass loading of 2.54 mg cm^{-2}. In particular, a reversible specific capacity of 1510 mAh g^{-1} is obtained on the basis of the total electrode weight and remains extraordinarily stable over 600 cycles, whilst the areal capacity is closely approaching the value of commercial lithium-ion batteries (3.9 mAh cm^{-2}). To the best of our knowledge, this is the first time that a Si anode with this level of performance has been described.

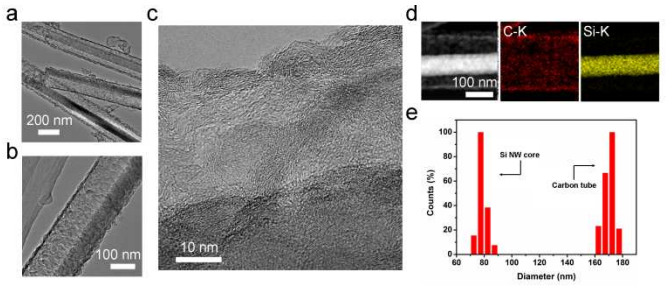

Fig. 3 The microstructure and uniformity of wt-Si/C nanocomposites in the array: (a-b) TEM and (c) high-resolution TEM images of wt-Si/C nanocomposites; (d) Carbon and silicon elemental mapping of a fraction of an individual wt-Si/C nanocomposite; (e) Statistical analysis of the diameter of Si NW cores and carbon tubes revealing the uniformity of wt-Si/C nanocomposites throughout the array.

The fabrication of wt-Si/C arrays involves uniform Si/C wire-in-tube nanostructuring and free-standing array manufacturing, and briefly comprises three steps (see more details in Experimental Section): (1) synthesis of uniform, vertically aligned silicon nanowires (Si NWs) on silicon wafers through a colloidal mask-sustained metal-assisted chemical etching method, (2) preparation of Si/C wire-in-tube nanocomposites by SiO_2 sacrificial layer-mediated processing, and (3) fabrication of free-standing wt-Si/C arrays via an alkaline-solution-enabled peeling process. As displayed in Fig. 2a, the peeled-off array remains the original modality with lateral sizes up to several centimeters. Such free-standing arrays are robust, thereby allowing for their direct integration as lithium-ion battery electrodes without introducing any auxiliary components.

The morphology and structure of as-produced wt-Si/C arrays are summarized in Fig. 2 and 3. As exhibited in Fig. 2b-d, the wt-Si/C nanocomposites in the array are well aligned and densely packed with an average diameter of ~170 nm and a typical length of ~60 μm. It is also shown that individual wt-Si/C nanocomposites are interconnected by an underlying thin layer as a hanging base, which is essential for maintaining the mechanical robustness and electrical conductivity of the free-standing array (Fig. S1, ESI). It should be noted that, although the typical areal mass loading of wt-Si/C arrays are around 2 mg cm^{-2} in this study, the loadings may be easily tuned, for example, by precisely controlling the mask size and subsequent processing conditions for Si nanowire synthesis and the scalability realized by recycling the used silicon wafers.[31] Furthermore, it is evident that each wt-Si/C nanocomposite in the array consists of an inner Si NW core, a hollow carbon tube, and the well-defined in-between void space that accommodates the volume change of silicon (Fig. 2d, 3a-d). The high-resolution transmission electron microscopy (TEM) image (Fig. 3c) discloses that the outer carbon tube (with a wall thickness of ca. 5 nm) possesses a turbostatic graphitic structure, consistent with the Raman spectroscopy and powder X-ray diffraction (XRD) results (Fig. S2, S3, ESI). Such thin and hollow carbon tubes are crucial for creating the internal voids to accommodate the volume change of silicon cores, providing paths for electron and ion transport from/to silicon, as well as blocking the direct contact of electrolyte and silicon and preventing the SEI propagation. It is noteworthy that our unique design is significantly different from previous reports of encapsulating nanostructured silicon with hollow carbon shells. The use of uniform Si NWs as starting materials (Fig. S4, ESI) promotes high uniformity of wt-Si/C nanocomposites in the array, in terms of the diameter of Si NW cores and carbon tubes (Fig. 3e), and thus ensures the formation of a well-defined void in each wt-Si/C nanocomposite so as to effectively accommodate the volume change of the Si NW core without rupturing the outer carbon tube.

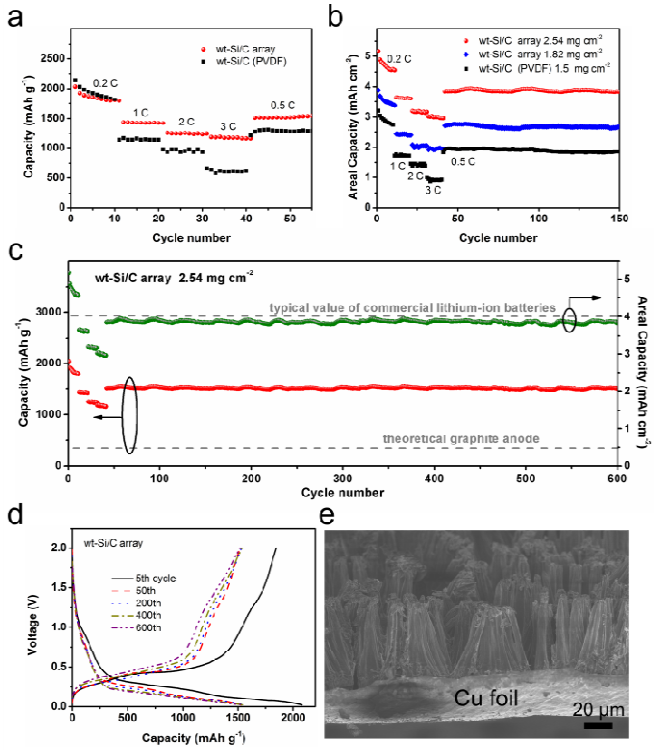

Fig. 4 Electrochemical characterization of wt-Si/C array electrodes: (a) Rate capabilities of wt-Si/C array and wt-Si/C (PVDF) electrodes from 0.2C to 3C (1C=3.6 A g^{-1}); (b) Areal capacities tested at different rates for two wt-Si/C array electrodes and a wt-Si/C (PVDF) control electrode; (c) Long-term cycling performance of the wt-Si/C array electrode with high areal mass loading of 2.54 mg cm^{-2}. The electrode was first cycled at different rates for initial 41 cycles and then 0.5C for later cycles; (d) Voltage profiles for a wt-Si/C array anode plotted for the 5th, 50th, 200th, 400th, and 600th cycles; (e) Typical SEM image of a wt-Si/C array after long-term cycling.

Considering a maximum Si volume change of up to 400% upon de(lithiation) processes, the diameter of outer carbon tubes (~170 nm) in this study was set to be approximately two times that of inner Si NWs (~80 nm) through tuning the thickness of SiO_2 sacrificial layers (Fig. 3e). The silicon content in the as-prepared wt-Si/C array was estimated to be around 74.4 wt% as determined by the thermogravimetry analysis (TGA, Fig. S5, ESI).

The unique structure of the designed wt-Si/C arrays affords remarkable battery performance. Two-electrode coin-type cells (2032) with metallic lithium counter electrodes were used to evaluate the electrochemical performance of wt-Si/C array electrodes, as well as wt-Si/C (PVDF) control electrodes (see Experimental Section). The typical mass loading of the wt-Si/C array electrodes was around 2 mg cm^{-2}; while in the wt-Si/C (PVDF) control electrodes, the active material mass loading was set to be approximately 1.5 mg cm^{-2}, which is an optimized maximum in our experiments if without sacrificing the integrity of the active material layer and subsequently cycling performances. Benefiting from the unique ordered configuration, the wt-Si/C array electrodes demonstrate high rate capability (Fig. 4a; Fig. S6, ESI). The specific capacity of the wt-Si/C arrays at the rates of 1C, 2C and 3C is 1421, 1244, and 1176 mAh g^{-1}, respectively, which is approximately 76, 66, and 63% of that at 0.2C. By

comparison, the wt-Si/C (PVDF) electrodes with a comparable active material mass loading level cannot match such capacity retention at higher rates, and show specific capacity of 1134, 929 and 602 mAh g^{-1} at 1C, 2C and 3C, respectively, which is 60, 48 and 32% of the 0.2C specific capacity. The excellent rate capability of the wt-Si/C array electrodes is attributed to their unique structure, where well-aligned wt-Si/C nanocomposites are mechanically and electrically interconnected by an underneath hinging layer, thus allowing for an uninterrupted, vertical, and fast transport of both electrons and lithium ions across the whole electrode thickness. This scenario is further verified by electrochemical impedance spectroscopy spectra (Fig. S7, ESI). Given that the exertion of every wt-Si/C nanocomposite in the array leads to 100% material utilization at all rates tested (Fig. S6b), the material utilization in the wt-Si/C (PVDF) electrode is comparable only at a smaller rate, and becomes in a rather low degree at higher rates (e.g., 50% of that in the wt-Si/C array at 3C). The low degree of material utilization can be associated with the intrinsic character of multi-interface electron transport between wt-Si/C nanocomposites as well as tortuous ion transport in the wt-Si/C (PVDF) electrodes which become sluggish and even interrupted when the material mass loading and thus electrode thickness increases.

Notably, a low degree of material utilization limits and even negates the potential of increasing the active material mass loading to improve the areal capacity.[20] With stable cycling as a requirement, a maximized areal capacity of 1.8 mAh cm^{-2} was achieved at a higher rate of 0.5 C for the wt-Si/C (PVDF) electrode with optimized areal mass loading of 1.5 mg cm^{-2} (Fig. 4b). In contrast, the areal capacity of the wt-Si/C arrays can be easily amplified and even reach the value of commercial lithium-ion batteries because of its flexibility in increasing electrode thickness and thus areal mass loading without introducing additional interfaces for electron and ion transport, as well as higher degree of material utilization. Specifically, the wt-Si/C arrays with areal mass loadings of 1.82 and 2.54 mg cm^{-2} deliver areal capacity of 2.7 and 3.9 mAh cm^{-2}, respectively, when being cycled at a rate of 0.5C (Fig. 4b). This implies that the areal capacity of the wt-Si/C arrays nearly depend linearly on their areal mass loadings, which can be highly favorable for further enhancements in areal capacity, if needed by specific applications such as micro-systems requiring high energy density per unit area. Furthermore, it was previously reported by us that the PVDF-enabled electrodes of nonuniform Si/C wire-in-tube nanocomposites showed stable cycling yet with continuous capacity fading over initial hundreds of cycles as well as at quite low areal mass loading of 0.2 mg cm^{-2}.[14] In contrast, over 100 cycles at 0.5C rate, the capacity retention is nearly 100% for the wt-Si/C array electrodes with areal mass loadings one order of magnitude higher than that of nonuniform Si/C nanocomposite-based ones (Fig. 4b). The stable cycling at such a mass loading level can be mainly attributed to the structural uniqueness and more importantly, uniformity of wt-Si/C nanocomposites. As reported widely for the design I, the well-defined internal void in a wt-Si/C nanocomposite allows for free expansion of the Si NW core without rupturing the outer carbon tube, thus enabling the structural and interfacial stabilization of the nanocomposite. The high uniformity of wt-Si/C nanocomposites in the array first guarantees every originally counted wt-Si/C nanocomposite building block to contribute to the capacity consistently without structural degradation, and second promotes electrode-level homogeneity whatever the active material mass loading level is, thus offering an explanation for the stable cycling of the array observed even at high mass loading. In addition, it has been generally recognized that even small variations induced by local inhomogeneity can accumulate across the electrode thickness and cause the electrode degradation.[23]

The synergistic engineering and control of structure, interface, and charge transport of the electrode turn out to be effective for long-term stable cycling of the wt-Si/C arrays with high mass loading. As exhibited in Fig. 4c, the wt-Si/C arrays show extraordinary cycling stability and almost invariably deliver specific capacity of 1510 mAh g^{-1} at a high rate of 0.5C over 600 cycles, which is more than four times beyond the theoretical capacity of graphite. More importantly, such high capacity and stable cycling are achieved at active material mass loading up to 2.54 mg cm^{-2}, which is one order of magnitude higher than those used in many publications, and is essentially needed to realize high-performance based on the total cell weight or volume. The areal capacity remains to be approximately 3.9 mAh cm^{-2} from the 42nd to 600th cycle at a rate of 0.5 C, which is rather close to the value of commercial lithium-ion batteries.[19,31,32] To the best of our knowledge, concurrently achieving high specific capacity on the basis of the total electrode weight, competitive areal capacity, and extraordinarily stable cycling with nearly 100% capacity retention at a high rate of 0.5C have seldom been reported for silicon anodes. This level of performance is thus among the best cycling performances of silicon anodes reported to date. Here, it should be noted that the estimated volumetric capacity (ca. 667 mAh cm^{-3}) is comparable to, if not greatly higher than, the volumetric capacity in commercial graphite anodes.[4,19,31,32-35] In addition, although the carbon tubes may contribute to the achieved capacity, the voltage profiles of wt-Si/C array electrodes exhibit typical electrochemical features of amorphous silicon, with negligible change over 600 cycles (Fig. 4d), which is consistent with the cyclic voltammetry measurements (Fig. S8, ESI). Moreover, the high average Coulombic efficiency of the wt-Si/C array electrodes from the 42nd to 600th cycles (99.7%), together with electrochemical impedance spectroscopy analyses after long-term cycling (Fig. S9, S10, ESI), further indicates the excellent structural and SEI control and the reversibility of the electrode reaction even at high material mass loadings enabled by our protocol of uniform Si/C wire-in-tube nanostructuring and free-standing array manufacturing. After being cycled, the structure and morphology of the wt-Si/C array are characterized further. It should be mentioned that the low Coulombic efficiency in the initial cycles (79% for the first cycle) can be mainly related to the irreversible trapping of lithium in the carbon tubes and the SEI formation (Fig. S9, S11, ESI); this may be improved by pre-lithiation processing.[36] As shown in Fig. 4e, the cycled wt-Si/C array retains an integrated membrane structure and the array height remains almost the same as the initial one (ca. 60 μm).

The geometry maintenance of the array observed implies the preservation of electron and ion transport paths in the cycled array, and the effectiveness of our design in silencing electrode-level variations of large volume change anode materials, which is crucial in developing a viable lithium-ion battery electrode. Furthermore, the modality of individual wt-Si/C nanocomposites remains after long-term cycling as confirmed by TEM and elemental mapping images (Fig. S12, ESI), which reflects the structural and interfacial stability of the wt-Si/C nanocomposites, contributing to the remarkable cycling stability of the wt-Si/C arrays.

Conclusions

In conclusion, we have demonstrated a novel Si anode design by uniform Si/C wire-in-tube nanostructuring and free-standing array manufacturing. Based on synergistic engineering and control of structure, interface and charge transport of the electrode, the as-developed free-standing, ordered arrays of uniform Si/C wire-in-tube nanocomposites, as a prototype of proof-of-concept anodes, exhibit unprecedented lithium storage performance at active material mass loadings one order of magnitude higher than that of most previous reports. In particular, a reversible specific capacity of 1510 mAh g^{-1} is obtained at a high rate of 1.8 A g^{-1} on the basis of the total electrode weight and remains extraordinarily stable with nearly 100% capacity retention at a high rate of 0.5C over 600 cycles, whilst the areal capacity is really approaching the value of commercial lithium-ion batteries (3.9 mAh cm^{-2}), thereby representing a substantial advance towards high-performance silicon anodes. While further performance enhancement can be based upon optimization of the diameter of silicon cores and the wall thickness of the carbon tubes, notably, the synergistic engineering and control of the electrode highlighted is applicable to the design and construction of other electrode materials especially facing large-volume-change electrode materials.

Acknowledgements

Financial support from the National Natural Science Foundation of China (Grants 21173057, 21273054, and 51302045), the Ministry of Science and Technology of China (2012CB933403) and the Chinese Academy of Sciences is acknowledged.

Notes and references

[a]*Key Laboratory of Nanosystem and Hierarchical Fabrication, National Center for Nanoscience and Technology, No. 11, Beiyitiao Zhongguancun, Beijing 100190, China. E-mail: lixl@nanoctr.cn; zhilj@nanoctr.cn*

† Electronic Supplementary Information (ESI) available: Experimental details and Figure S1-S12. See DOI: 10.1039/c000000x/

1 N. S. Choi, Z. H. Chen, S. A. Freunberger, X. L. Ji, Y. K. Sun, K. Amine, G. Yushin, L. F. Nazar, J. Cho and P. G. Bruce, *Angew. Chem. Int. Ed.*, 2012, **51**, 9994.
2 H. Wu, G. Chan, J. W. Choi, I. Ryu, Y. Yao, M. T. McDowell, S. W. Lee, A. Jackson, Y. Yang, L.B. Hu and Y. Cui, *Nat. Nanotechnol.*, 2012, **7**, 310.
3 H. Li, X. Huang, L. Chen, Z. Wu and Y. Liang, *Electrochem. Solid State Lett.*, 1999, **2**, 547.
4 A. Magasinski, P. Dixon, B. Hertzberg, A. Kvit, J. Ayala and G. Yushin, *Nat. Mater.*, 2010, **9**, 353.
5 J. Y. Luo, X. Zhao, J. S. Wu, H. D. Jang, H. H. Kung and J. X. Huang, *J. Phys. Chem. Lett.*, 2012, **3**, 1824.
6 J. Chang, X. Huang, G. Zhou, S. Cui, P. B. Hallac, J. Jiang, P. T. Hurley and J. Chen, *Adv. Mater.*, 2014, **26**, 758.
7 L. B. Hu, H. Wu, Y. F. Gao, A. Y. Cao, H. B. Li, J. McDough, X. Xie, M. Zhou and Y. Cui, *Adv. Energy Mater.*, 2011, **1**, 523.
8 B. Wang, X. Li, T. Qiu, B. Luo, J. Ning, J. Li, X. Zhang, M. Liang and L. Zhi, *Nano Lett.*, 2013, **13**, 5578.
9 J. W. Deng, H. X. Ji, C. L. Yan, J. X. Zhang, W. P. Si, S. Baunack, S. Oswald, Y. F. Mei and O. G. Schmidt, *Angew. Chem. Int. Ed.*, 2013, 52, 2326.
10 M. Ge, Y. Lu, P. Erius, J. Rong, X. Fang, M. Mecklenburg and C. W. Zhou, *Nano Lett.*, 2014, **14**, 261.
11 N. Liu, H. Wu, M. T. McDowell, Y. Yao, C. M. Wang and Y. Cui, *Nano Lett.*, 2012, **12**, 3315.
12 X. L. Li, P. Meduri, X. L. Chen, W. Qi, M. H. Engelhard, W. Xu, F. Ding, J. Xiao, W. Wang, C. M. Wang, J. G. Zhang and J. Liu, *J. Mater. Chem.*, 2012, **22**, 11014.
13 S. Chen, M. L. Gordin, R. Yi, G. Howlett, H. Sohn and D. Wang, *Phys. Chem. Chem. Phys.*, 2012, **14**, 12741.
14 B. Wang, X. Li, X. Zhang, B. Luo, Y. Zhang and L. Zhi, *Adv. Mater.*, 2013, **25**, 3560.
15 X. Li and L. Zhi, *Nanoscale*, 2013, **5**, 8864.
16 S. Ohara, J. Suzuki, K. Sekine and T. Takamura, *J. Power Sources*, 2004, **136**, 303.
17 X. Li, J. H. Cho, N. Li, Y. Y. Zhang, D. Williams, S. A. Dayeh and S. T. Picraux, *Adv. Energy Mater.*, 2012, **2**, 87.
18 M. F. L. De Volder, S. H. Tawfick, R. H. Baughman and A. J. Hart, *Science*, 2013, **339**, 535.
19 N. Liu, Z. Lu, J. Zhao, M. McDowell, H. Lee, W. Zhao and Y. Cui, *Nat. Nanotechnol.*, 2014, **9**, 187.
20 R. Yi, J. Zai, F. Dai, M. L. Gordin and D. H. Wang, *Nano Energy*, 2014, 6, 211.
21 R. Yi, F. Dai, M. L. Gordin, S. Chen, D. Wang, *Adv. Energy Mater.*, 2013, **3**, 295.
22 L. Taberna, S. Mitra, P. Poizot, P. Simon and J. M. Tarascon, *Nat. Mater.*, 2006, **5**, 567.
23 S. J. Harris and P. Lu, *J. Phys. Chem. C*, 2013, **117**, 6481.
24 S. C. Zhang, Z. J. Du, R. X. Lin, T. Jiang, G. R. Liu, X. M. Wu and D. S. Weng, *Adv. Mater.*, 2010, **22**, 5378.
25 X. L. Chen, K. Gerasopoulos, J. C. Guo, A. Brown, C. S. Wang, R. Ghodssi and J. N. Culver, *ACS Nano*, 2010, **4**, 5366.
26 Y. Yao, K. F. Huo, L. B. Hu, N. A. Liu, J. J. Ha, M. T. McDowell, P. K. Chu and Y. Cui, *ACS Nano*, 2011, **5**, 8346.
27 F. F. Cao, J. W. Deng, S. Xin, H. X. Ji, O. G. Schmidt, L. J. Wan and Y. G. Guo, *Adv. Mater.*, 2011, **23**, 4415.
28 K. Evanoff, J. Khan, A. A. Balandin, A. Magasinski, W. J. Ready, T. F. Fuller and G. Yushin, *Adv. Mater.*, 2012, **24**, 533.
29 A. Gohier, B. Laik, K. H. Kim, J. L. Maurice, J. P. Pereira-Ramos, C. S. Cojocaru and P. T. Van, *Adv. Mater.*, 2012, **24**, 2592.
30 G. Kim, S. Jeong, J. Shin, J. Cho and H. Lee, *ACS Nano*, 2014, **8**, 1907.
31 A. Vlad, A. L. M. Reddy, A. Ajayan, N. Singh, J. F. Gohy, S. Melinte and P. M. Ajayan, *Proc. Natl. Acad. Sci. U.S.A.*, 2012, 109, 15168.
32 J. W. Choi, L. B. Hu, L. F. Cui, J. R. McDonough, and Y. Cui, *J. Power Sources*, 2010, 195, 8311.
33 R. Moshtev, and B. Johnson, *J. Power Sources*, 2000, 91, 86.
34 I. Kovalenko, B. Zdyrko, A. Magasinski, B. Hertzberg, Z. Milicev, R. Burtovyy, I. Luzinov, and G. Yushin, *Science*, 2011, 334, 75.
35 S. Jeong, J. Lee, M. Ko, G. Kim, S. Park, and J. Cho, *Nano Lett.*, 2013, 13, 3403.
36 N. Liu, L. Hu, M. T. McDowell, A. Jackson, and Y. Cui, *ACS Nano*, 2011, 5, 6487.

TOC

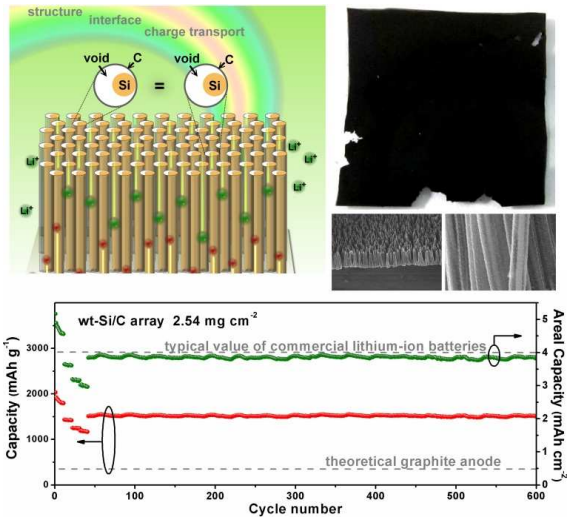

Self-standing, ordered arrays of uniform Si/C wire-in-tube nanocomposites are developed, showing high specific capacity and extraordinary cycling stability whilst delivering competitive areal capacity.